Journal of Non-Crystalline Solids 690 (2026) 124214

Contents lists available at ScienceDirect

Journal of Non-Crystalline Solids

journal homepage: www.elsevier.com/locate/jnoncrysol

Model of convective drying of Resorcinol-Formaldehyde gels to xerogels

Lorenz Ratke [a],*, Benjamin Ignatzi [b]

[a] Retired Dep.Head, Institute of Materials Research, German Aerospace Centre, DLR, Haberstrasse 17, Sankt Augustin, 53757, NRW, Germany
[b] Institute of Frontier Materials on Earth and in Space, German Aerospace Centre, DLR, Linder Hoehe, Cologne, 51147, NRW, Germany

ARTICLE INFO

Keywords:
Drying
Convective diffusion
Aerogels
Xerogels

ABSTRACT

Drying of a wet gel with an inherent fractal solid nanostructure and pores of mesoscale sizes is a complicated process of evaporation of the pore liquid, a visco-elastic and visco-plastic response the solid network, gas transport at the gel surface and transport through the pores. In this paper an analytical model is derived that takes into account convective–diffusive transport in a drying cabinet and permeation through the pore space. The analytical model neglects any deformation of the solid network. It only calculates the gas transport. The model is compared with experimental results obtained by drying of resorcinol-formaldehyde gels in a drying cabinet having a fan. The agreement between experiments and model is good in light of the simplifications made and thus allows to calculate drying time for various sample geometries and flow characteristics expressed by Reynolds number.

1. Introduction

Aerogels are typically prepared by sol–gel methods [1,2] leading in a first step to a wet gel, which must be dried to get a mesoporous solid with a huge specific surface area, low thermal conductivity, low envelope density and other outstanding properties. Drying is either performed supercritically with carbondioxide, quite often after a solvent exchange or simply by evaporation of the pore liquid, solvent, in a drying cabinet. Drying of a wet gel under ambient conditions or at slightly higher temperature, below the boiling point of the solvent mixture, leads typically to so-called xerogels, because the original solid particle or fibre network in the wet gels most often shrinks drastically leading to a much reduced porosity less than 50%. The drying process is in many cases recorded simply by continuous weighing of the sample. Such mass loss curves are modelled using for instance kinetic theory of gases, description of transport processes of the pore liquid to the surface through the pore space treating pores as tubes and using Hagen–Poiseuille law for fluid and gas transport, deformation of the solid network by the action of capillary forces driving the fluid out of the pore space or simply by a diffusion approach as originally proposed by Crank in his textbook on diffusion [3] and used by Bisson and co-workers to describe the drying of wet silica gels whose pore surfaces were made hydrophobic [4]. Interesting enough, evaporative drying has never been a serious subject of research in the aerogel research during the last decades. There are only a few exceptions. Brinker and Scherer devote a whole chapter to drying [2] as well as recently Ratke and Gurikov [1]. They both review the state of the art at their time, but also conclude that no theoretical development has taken place to account for the specialities of mesostructured gels, namely their huge pore space (around 90 to 99%) built of a network of particles ranging from a few ten nanometers to around a micron.

Fricke and co-workers found in the late 90s of last century [5,6] that Resorcinol-Formaldehyde (RF) gels can be dried by evaporation of the solvent if the molar ratio of resorcinol to catalyst (typically sodium carbonate) is higher than approximately 1000. Then so-called ambient drying leads to aerogels with a porosity around 80 to 90% and almost negligible shrinkage (for more details see [1] and the chapter on drying therein). Drying, meaning the evaporation of the solvent, can be enhanced by air convection in a drying cabinet having a suitable ventilator. Especially Haghighi [7] investigated theoretically the drying of wet soils under turbulent airflow conditions above the soil, diffusive transport in the pore space, and also took into account the temperature variation due to evaporation. Convective-diffusive drying of mesostructured wet gels was, as to our knowledge, never investigated theoretically. The aim of this paper is to show with simple considerations and easy-to-apply equations how convection in a drying cabinet affects the drying time and how it scales with the size or shape of the wet gel. The model developed is compared with experimental results on RF-gels.

2. Mass loss

Let us start with a few simple considerations: how drying of a wet gel can be measured and recorded. The simplest way to monitor drying

* Corresponding author.
E-mail address: lorenz.ratke@gmx.de (L. Ratke).

https://doi.org/10.1016/j.jnoncrysol.2026.124214
Received 23 February 2026; Received in revised form 17 May 2026; Accepted 24 May 2026
Available online 30 May 2026

is to measure continuously its mass (or better, weight). This is most easily done by a digital balance operating in a drying cabinet. The gel shall initially have the mass $m_G(0)$, which changes with time t such that $m_G(t)$. The wet gel shall be placed in a container having a mass m_c. If the gel is fully dried, the residual mass is that of the aerogel m_A. During the measurement the mass of the gel continuously varies.

$$m(t) = m_G(t) + m_c \tag{1}$$

Initially we have

$$m_0 = m(0) = m_G(0) + m_c \tag{2}$$

The gel consists of a solid network with the mass m_A and a fluid in the pore space, whose mass is m_F. We then have

$$m_G(t) = m_A + m_F(t) \tag{3}$$

The pore liquid evaporates at the surface of the gel, and the gas is transported into the space above the gel body. Capillary forces pull the pore liquid continuously to the surface such that a constant source for vapour exists. The pulling action is counterbalanced by the viscoelastic deformation of the solid network until it cannot withstand any more stress and either the liquid moves into the pores and the liquid–gas interface (meniscus) is inside the solid network or the gel breaks into pieces (as is often observed in silica gels based on water glass during evaporative drying). In RF-gels synthesised with a low catalyst concentration, such that the Resorcinol-Catalyst ratio, RC, value is above 1000 (for more details see [1]), the gel body stays intact and the menisci move into the solid network of RF-particles. Then the evaporation mechanism changes since now the vapour must be transported through the pore network, which goes either via permeation or diffusion. Till this critical point the weight or mass loss decreases linearly with time [2], meaning the time derivative is constant.

$$\frac{dm_G(t)}{dt} = \frac{dm(t)}{dt} = \frac{dm_F(t)}{dt} = \text{constant} \tag{4}$$

This period of drying is therefore called in the literature the constant rate period (CRP). Quite often in the literature not the absolute mass loss is reported but a relative one. There are many ways to do this. In this study we used the fluid loading, defined as

$$r_4 = \frac{m_F}{m_A} \tag{5}$$

with $r_4(t=0) = m_F(0)/m_A > 1$ and $r_4 = 0$ after complete drying as also done by Bisson et al. [4] for silica gels. The total mass loss rate dm/dt could easily be calculated by differentiating the mass with respect time. This especially simple since modern electronic balances allow to take a huge number of data points with small time intervals.

3. Mass loss rate

Let us first make a simple consideration about the mass loss rate of the pore liquid. At the surface of the wet gel there always exists a fluid layer as long as the capillary forces are able to pull liquid to the sample's surface. This is especially true in gels with a pore volume of larger than 80% and a solid network consisting of particles with diameters between 10 and 100 nm. If pore sizes are in a submicron range, the capillary forces are in the range of a few 10 MPa.

These forces induce a fluid flow, which can be described in macroporous materials as a Hagen–Poiseuille flow or is better described by the Darcy equation. This is extensively discussed in the literature for many types of porous materials; see for instance [7–11]. In almost all literature on drying of wet porous materials, the solid network is usually taken as fixed and not deformable. As pointed out by Scherer, in reality the solid network in gels reacts during drying with deformation. It is shrinking, and the fluid flow is directed opposite to it. From the liquid inside the pores and the surface layer, evaporation takes place, which can be calculated, for instance, with the kinetic theory of gases as

$$Z = \alpha M \frac{p(T) - p_a}{\sqrt{2\pi M RT}} \tag{6}$$

This rate Z has the units kg/(m^{2}s). $p(T)$ is the vapour pressure at temperature T, M the molar mass in kg/mol, R the universal gas constant and p_a the gas pressure far away from the wet gel. α is a factor typically below one [12]. If the evaporating surface has the area A, we can write for the evaporating mass m_g the equation

$$\frac{dm_G}{dt} = -Z \cdot A \quad \text{or} \quad m_G(t) = m_0 - Z \cdot A \cdot t \tag{7}$$

We rewrite this equation a bit using $m_0 = \rho_L A \cdot h$, with ρ_L as the density of the pore liquid and h as the sample thickness.

$$\frac{m_G(t)}{m_0} = 1 - \frac{Z}{\rho_L h} \cdot t \tag{8}$$

The time when drying is completed, t_e is then

$$t_e = \frac{\rho_L h}{Z} \tag{9}$$

For typical sample thicknesses of a few centimeters, taking water as the pore liquid, drying times of only a few seconds are calculated being thus orders of magnitude away from reality. Eqs. (6) and (7) are quite often generalised by simply writing, as done by Brinker and Scherer [2] and many others, for the volumetric gas evaporation rate

$$\frac{dV_g}{dt} = k(p(T) - p_a) \tag{10}$$

introducing an empirical proportionality constant k. The essential idea in this equation is that the evaporation rate is proportional to the driving force, the pressure difference. Many approaches in the literature on drying of packed beds, porous rocks, sand pillars, wet soils, and other open porous materials [7,13–16] use this equation and model the proportionality constant. An excellent modelling was done by Haghighi in his PhD thesis [7] for turbulent airflow above a wet soil using a turbulent boundary layer approach and allowing for diffusion of the evaporating gas through the pore space. In a recent paper, Weichel and co-workers [17] discuss drying of porous battery materials using a multi-phase field approach. They treat fluid flow inside the pore network with a suitably formulated Navier–Stokes equation, adding a capillarity term, and the evaporation at the liquid–gas interface is treated as a phase transition. The evaporation rate is considered constant. Their numerical results show that drying is not uniform in a bed of irregularly shaped grains but is inhomogeneous, meaning completely dry paths can exist in parallel with still wet areas, as already discussed by Prat and co-workers [14]. They, however, neglect the transport process in the space above the wet porous solid.

In contrast to such complex numerical models, we first develop here a simple model to catch essential physics, and second we focus on the evaporation process at the surface and inside the pores and do not treat the evaporation process as constant in time. Brinker and Scherer, in their seminal book on sol–gel processing, use Eq. (10) for the evaporation at the surface with a constant proportionality factor. They concentrate on the gel network response during drying and the viscoelastic and viscoplastic deformation of the solid network. These ideas are taken up today to treat the microstructural response of battery electrode materials during drying [18,19]. In our simple model of drying we neglect the gel's elasto-plastic response. This serious simplification will be discussed at the end.

4. Transport in the gas space

In this section we will discuss the evaporation at the sample surface in the so-called constant rate period (CRP) and compare the results with experimental measurements of the drying curves in the range where $dm/dt = const$.

4.1. Modelling of convective-diffusive evaporation

When all gas molecules leaving the gel surface would rapidly be removed from it into the space above the gel body (which happens only if above the body a vacuum would exist). Comets are an example of sublimating into vacuum, then one could use Eq. (8) to calculate the mass as a function of time. Reality in a drying cabinet is, however, not that simple. One has to take into account that a molecule leaving the gel surface will on average collide with molecules in the gas space above the surface within a mean free paths, being around a hundred nanometers. Such collision events might even lead to a rebouncing of molecules to the surface, and even re-condensation is possible. We therefore might assume that within a small layer above the surface quickly a gas layer establishes, having a thickness of several mean free path, the so-called Knudsen layer [12]. We assume that in this layer the gas concentration is identical with the concentration given by the evaporation line, $p_{sat}(T)$, in the phase diagram (at constant temperature), see [7]. This saturation concentration, measured in mol/volume $c_s = p_{sat}(T)/RT$, is fixed, and any concentration difference to the gas phase above the gel body determines the evaporation rate and the mass loss. The thin gas layer at the surface is refilled with the evaporation rate $Z(T)$. We also always assume isothermal conditions and thus neglect heat transfer. In general, drying is much more complex, since one also has to take into account that evaporation leads to cooling of the gel body; see Whitaker [20,21].

Typically in a drying cabinet there is a fan which drives gas flow above samples to homogenise the temperature field in a drying cabinet. The convective air flow influences the drying kinetics. Assume for simplicity that there exists a flow with a velocity $u(x)$ parallel to the wet gel surface with x a coordinate perpendicular to the gel surface. Then the diffusion equation reads in one dimension

$$\frac{\partial c}{\partial t} = D_g \frac{\partial^2 c}{\partial x^2} + \frac{\partial}{\partial x}(u(x)c) \tag{11}$$

A solution of this equation requires knowledge of the flow field $u(x)$, which can be obtained from a solution of the Navier–Stokes equation. Instead of solving the real coupled problem of gas flow and diffusion, we make a simple, so-called boundary layer approach [22]. Far away from the sample, the gas flow shall have a constant velocity u_0. At the sample surface the flow velocity is zero due to the no-slip boundary condition. Therefore two boundary layers exist. First the so-called hydrodynamic layer with a width δ_0 and second a diffusive layer with a thickness δ. The diffusion boundary layer is usually thinner than the hydrodynamic Prandtl layer. The way both layers depend on the gas flow is already solved in the literature [23]. Since outside the diffusion boundary layer the concentration $c_a = p_a/(RT)$ is constant it is allowed to simplify the mass flow from the surface in the following way

$$j = -D_g \frac{c_s - c_a}{\delta} \tag{12}$$

Here c_s is the concentration in the Knudsen layer. Such an approach was already used by [7,24] and Castell et al. [25] for wet soils. The mass loss rate is calculated with M the molar mass of the evaporating liquid

$$\frac{dm}{dt} = MAj = -MAD_g \frac{c_s - c_a}{\delta} \tag{13}$$

with A as the sample surface. As long as c_s is constant one can integrate this equation yielding

$$m(t) = m_0 - MAD_g \frac{c_s - c_a}{\delta} t \tag{14}$$

The mass reduces linear with time in agreement with experiments. The only item for which we need an expression is the boundary layer thickness δ. The literature cited gives expressions for both layers, which are adopted here to take into account that outside the sample there is a gas flow. For gases we have that the Schmidt number is always $\mathrm{Sc} = \nu/D_g = 1$ since the kinematic viscosity ν and the diffusion coefficient are equal. Using this relation, we get

$$\delta = \delta_0/\mathrm{Sc}^{1/3} = \delta_0 \tag{15}$$

The hydrodynamic boundary layer thickness is in the laminar case (the critical Reynolds number for flow above a flat surface is around 500 000)

$$\delta_0 = 5\frac{L}{\sqrt{Re}} \tag{16}$$

with L as the lateral extension of the sample. In principle the layer is not of constant thickness but varies along the length of the sample. At the edge, $x = 0$, the layer thickness is zero and increases with distance from the edge. The airflow in a drying cabinet is probably not a simple flow parallel to a sample surface, but here we use such a simplification. Reynolds number is defined as

$$\mathrm{Re} = \frac{u_0 L}{\nu} \tag{17}$$

with u_0 as the flow velocity. Inserting this expressions into Eq. (14) yields for the mass loss under laminar conditions

$$m(t) = m_0 - MAD_g \frac{c_s - c_a}{5L}\sqrt{\mathrm{Re}} \cdot t \tag{18}$$

With increasing flow velocity or Reynolds number the drying would run faster. Fig. 2 shows a calculation of the linear drying according to Eq. (18) under laminar flow conditions. The figure clearly shows that with increasing Reynolds number or flow velocity the drying becomes faster, as expected. The horizontal plane marks that the mass loss is complete, meaning $m(t) = 0$. The intersection with the drying curve follows a square root law according to Eq. (18). It also shows that a typical drying time would be of the order of 50,000 to 100,000 s or around a day. The values are in full agreement with daily experience and especially with experimental data shown and discussed below. Assume that a sample could fully dried by convective diffusion. Then we could calculate the time t_e needed for it by setting $m(t_e) = 0$.

$$t_e = \frac{5Lm_0}{AMD_g\sqrt{Re}(c_s - c_a)} = \frac{5L\rho_L\phi_p \cdot h}{MD_g\sqrt{Re}(c_s - c_a)} = q(T) \cdot h \tag{19}$$

where we have used that $m_0 = \rho_L V\phi_p + \rho_s V\phi_s = A \cdot h(\rho_l\phi_p + \rho_s\phi_s) \cong \rho_L A \cdot \phi_p \cdot h$ with ϕ_p, ϕ_s the volume fractions of pores and solid. The relation $t_e = q(T)\,h$ and the linear decrease in mass with time, Eq. (14), allow an experimental test (see Fig. 1).

4.2. Experimental procedures

We dried RF-gels, which were catalysed with sodiumcarbonate (R/C = 1500) such that evaporative drying was possible without any crack formation. Resorcinol was dissolved in deionised water (R/W = 0.044), an aqueous solution of formaldehyde with 23.5% formaldehyde was added (R/F = 0.74) and finally sodiumcarbonate. The pH of the solution was adjusted with nitric acid to a value of 5.4–5.6. The sample had a size of 13.2 cm times 13.2 cm with variable thickness. The gelling solution was put into a container, which was sealed, kept in the container for 48 h at 80 °C in the drying cabinet UF260 plus from Memmert, which allows to control the ventilation in 10 steps. The ventilated air is preheated to the desired temperature. The fan run at $N = 2640$ rpm and had a radius of $R = 75$ mm. The tip velocity is $U_{\mathrm{tip}} = 2\pi NR/60$. The Reynolds number calculated from the tip velocity is around 67 000 using the kinematic viscosity of air. Once the designed temperature was achieved the containers were opened while in the drying cabinet, such that the samples were kept at constant temperature. The drying was monitored with a digital balance, Innovateking with an accuracy of ±1 g. The mass change was recorded every two seconds and then the values were averaged in 10 min intervals. Shrinkage was measured after complete drying by simply measuring the dimensions of the samples. The envelope density was measured with

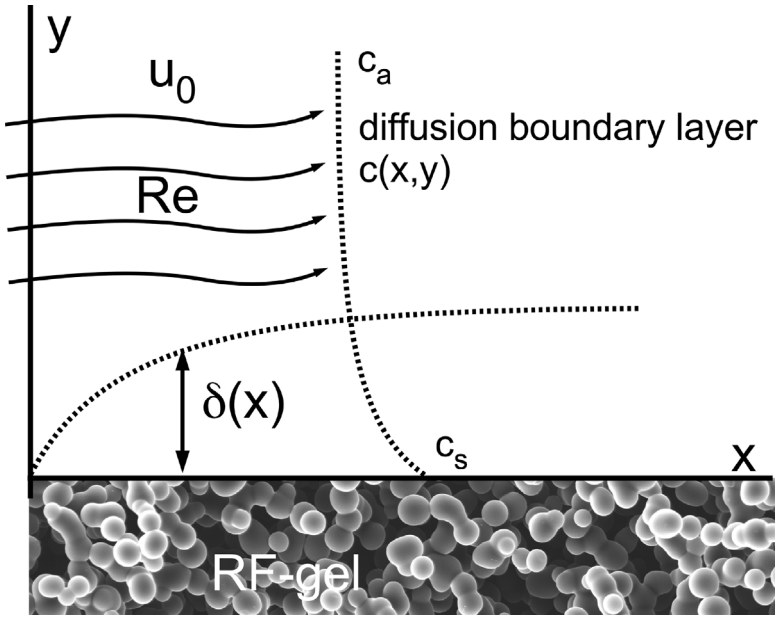

Fig. 1. Scheme of the diffusion boundary layer above an RF-gel. The boundary layer increases in thickness starting from the edge in the direction of air flow indicated by the flow velocity u_0 or its Reynolds number Re.

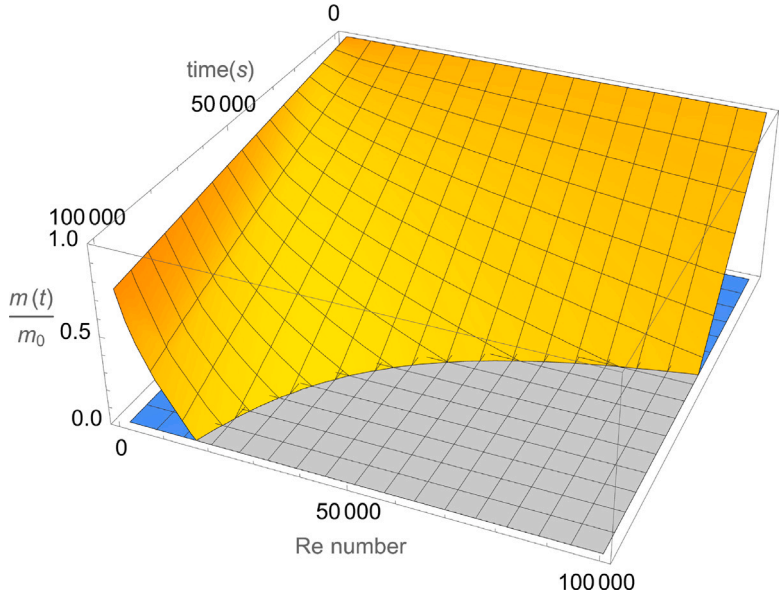

Fig. 2. Theoretical drying time for various Reynold's numbers after Eq. (18). For the calculation it is assumed that the gel fluid is water. The vapour pressure of water at 80 °C is 500 hPa, the sample thickness is h = 30 mm, the diffusion coefficient in the gas phase is assumed to be that of air 15.4 · 10^{-6} m^2/s, the sample surface is 0.0169 m^2 and the characteristic length L is set as 0.4 m - parameters fit to the experimental conditions. The water vapour pressure far away from the sample surface is set to 100 Pa (dry air).

the GeoPyc 1360 equipment and the skeletal one measured with the Accupyc 1340, both from Micromeretics. The porosity varied slightly with temperature being 79.4 ± 1.2 % at 80 °C, 79.5 ± 0.7% at 70 °C and 79.7 ± 0.65% at 60 °C. The envelope density was 0.29 ± 0.01 g/cm^3 independent of the drying temperature and the skeletal densities were around 1.43 ± 0.03 g/cm^3. Typically in RF aerogels the skeletal density is around 1.55 g/cm^3 [1] and thus one might conclude that the particles in these aerogels are not dense but itself porous, probably have some microporosity. The observed shrinkage was 2.2% in the lateral directions. No shrinkage was measured in the thickness direction. The volume shrinkage is in all samples 4.5%. The specific surface area was measured with nitrogen adsorption at 77 K with the TriFlex facility of Micromeretics taking a seven point adsorption isotherm. The average specific surface area was 0.74 ± 0.08 m^2/g. Since SEM pictures, see Fig. 3, show that the particles are spherical the average particle diameter can be estimated from the specific surface area to be 2.4 μm. The average pore size is then around 5.5 μm and thus the average Knudsen number Kn = 0.014. This is around a factor of 100 smaller than in super-critically dried RF aerogels; for details see [1]. From these experimental data we conclude that the pore space in these xerogels after drying is macroporous. We therefore develop below a model for convective transport in the pore space being determined by Darcy's law

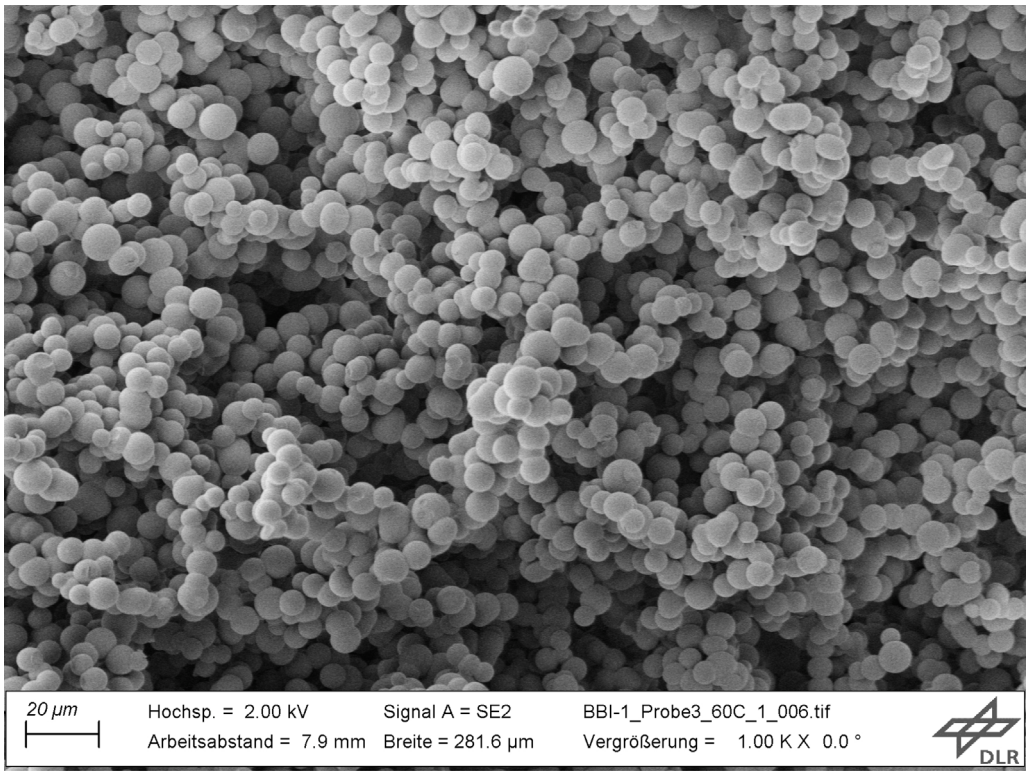

Fig. 3. SEM picture of an RF aerogel dried at 60 °C showing that the particle in the network are spherical. They all have a similar size.

using either for the permeability a Knudsen approach for mesoporous or a classical Kármán–Kozeny one for macroporous materials.

4.3. Comparison with experimental data

The recorded drying curves and their interpretation is discussed in the following sections. All experimental details are in [26]. Fig. 4 shows drying curves for samples with different thicknesses. The variation of drying with temperature for a fixed thickness of 30 mm is shown in Fig. 5. It is obvious that with increasing temperature the drying time decreases. There also is another interesting point: At the beginning of drying there is a rapid decreases in mass before the linear decrease sets in. Performing a least square fit to the linear part of the drying curves with Eq. (18) excluding the first two or three points and then extrapolating the linear part to zero mass yields values of t_e. If the model outlined above is right, this time should be proportional to the sample thickness. Fig. 6 shows the result. The agreement between experiment and model is acceptable, especially for the drying temperatures of 70 and 80 °C. In the data for drying at 60 °C the point at 20 mm sample thickness does not follow the expected behaviour. Comparing the slopes of the linear part of the drying curves with the theoretical prediction of Eq. (14), using the Reynolds number given by the fan data leaves the characteristic length of the boundary layer as the only variable. The numerical analysis shows that the characteristic length would vary between 0.02 m and 0.7 m and thus would be around the size of the drying cabinet.

Let us take a look at the temperature dependence of the pre-factor in Eq. (19)

$$q(T) = \frac{5L\,\rho_L\phi_p}{M\,D_g\sqrt{Re}(c_s(T) - c_a)} \tag{20}$$

It is driven by the temperature dependence of the diffusion coefficient and that of the vapour pressure or vapour concentration. The diffusion coefficient is in the small temperature range considered constant, but the vapour concentration is exponentially dependent on temperature according to Antoine's law (Clausius–Clapeyron equation). Doing first a linear fit to the data points in Fig. 6, extracting the slope $q(T)$ and then performing a fit with $\exp(-Q/RT)$ leads to Fig. 7. It shows that the slope q follows the expected trend, namely, it decreases with temperature, and the assumed model fits well to the data. The driver of the temperature dependence of drying time is therefore essentially the strong temperature dependence of vapour pressure. The energy for vaporisation Q from this fit is around 40 kJ/mol and thus in the order the vaporisation enthalpy of water.

Although the fits to experimental data support the model behind it, the agreement between experiments and model should not overvalued, since the data base is rather small and the air dynamics in the drying cabinet are probably more complex than a simple parallel flow above the samples.

4.4. Final stage of drying

Once the liquid–gas interfaces have entered the pore space, the transport of evaporating pore liquid changes to a transport through the meso- to nanoscale pores. This is called the falling rate period (FRP), since the mass loss rate decreases with time and slowly levels off to zero. Fig. 8 illustrates this situation. We develop a simple model describing the mass loss in this stage. Assume that the liquid–gas interfaces are drawn into the solid network by an amount $y(t)$, on average. Then the pore liquid evaporates still in the same manner as described by Eq. (6), meaning there still is a saturation gas layer with concentration c_s, but the transport to the sample surface and the gas space in the drying cabinet occurs by permeation or Knudsen diffusion. For the sake of simplicity, assume first that the menisci are described as shown in Fig. 8. We later replace this assumption with a better one, reflecting that the liquid wets the solid network and therefore the solid–liquid interface is curved.

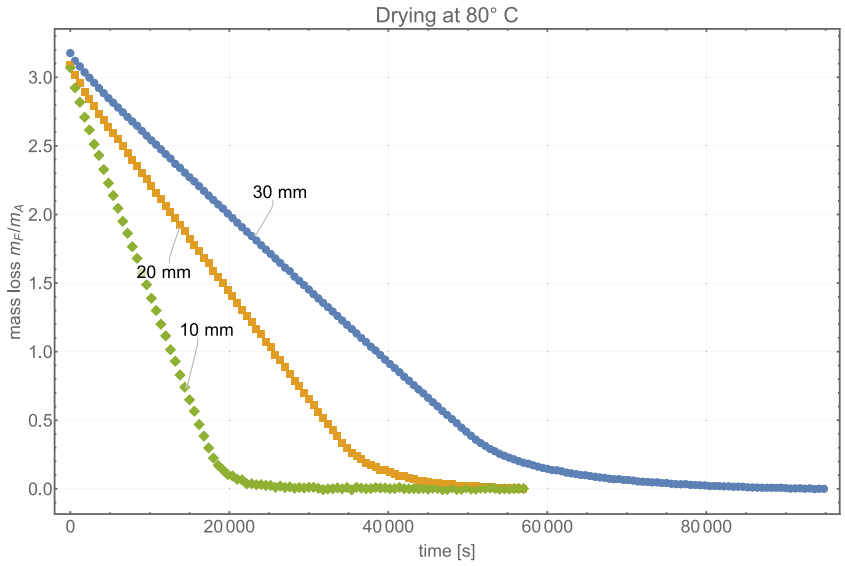

Fig. 4. Drying curve of RF-gels kept at 80 °C with three different thicknesses. Plotted is here r_4, the ratio of pore liquid to the final dry mass of the sample.

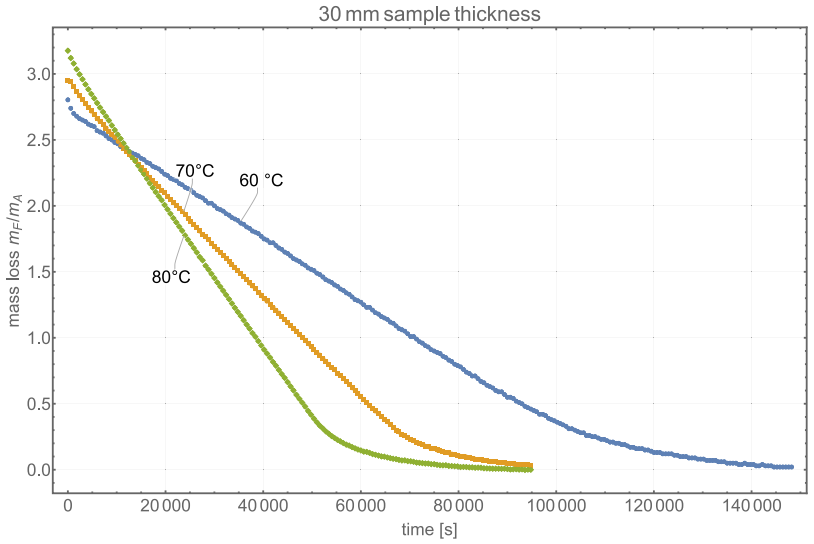

Fig. 5. Drying curve of RF-gels with a sample thickness of 30 mm for three different temperatures. Plotted is here r_4, the ratio of pore liquid to the final dry mass of the sample.

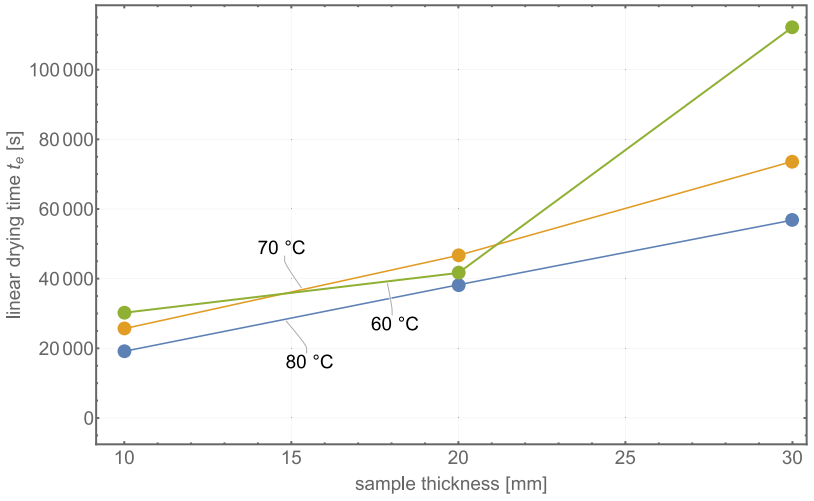

Fig. 6. The extrapolated drying time t_e, see Eq. (19) as a function of sample thickness for three different temperatures.

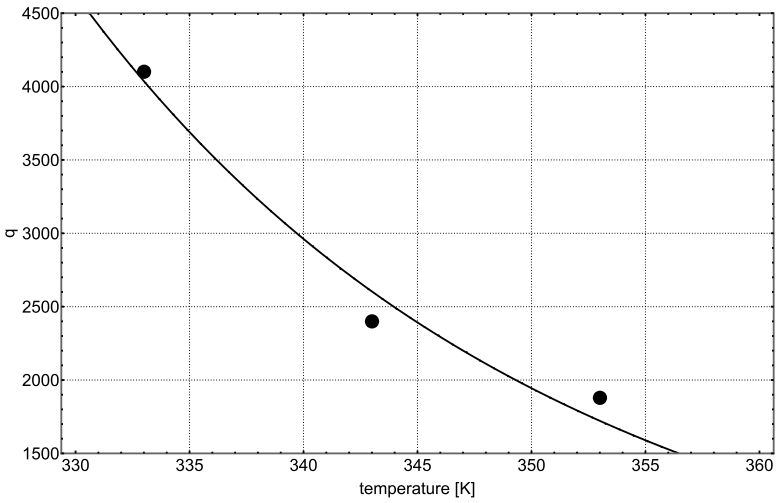

Fig. 7. Slope of Eq. (19) decreasing with drying temperature. The decrease is mainly caused by the temperature dependence of the vapour concentration in the Knudsen layer or its counterpart, the vapour pressure of the pore fluid.

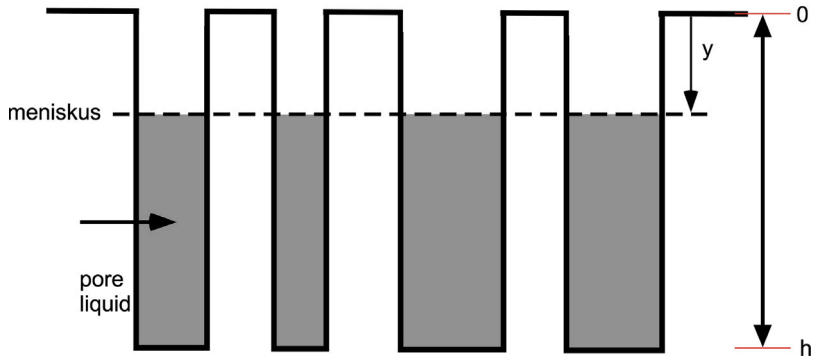

Fig. 8. Illustration of the liquid–gas interface (menisci) being drawn into the porous body by an amount $y(t)$.

4.5. Permeation through the pore space

If the transport of evaporated gas can be described as a permeation process, we can apply Darcy's law. The velocity v of the gas can be calculated

$$\mathrm{v} = -\frac{K}{\mu}\nabla p \tag{21}$$

with K as the permeability of the network and μ as the dynamic viscosity of the gas. The pressure gradient is simplified as

$$\nabla p \cong \frac{p - p_a}{y} = \frac{\Delta p}{y} \tag{22}$$

The total mass flux through the pores occupying an area $A_p = \phi_p A$, with A as the sample surface area and ϕ_p the pore volume fraction.

$$\frac{dm}{dt} = A_p \rho_g v = -A_p \rho_g \frac{K}{\mu}\frac{p - p_a}{y} \tag{23}$$

In order to solve this equation we have to find an expression for $y(t)$. This is done as follows. The total mass loss rate can also be written as

$$\frac{dm}{dt} = \rho_L \frac{dV_L}{dt} = A_p \rho_g v \tag{24}$$

The volume of the pore liquid is $V_L = A_p(h - y)$ and thus

$$\frac{dV_L}{dt} = -A_p \frac{dy}{dt} \tag{25}$$

This allows to derive a differential equation for $y(t)$

$$-\rho_L A_p \frac{dy}{dt} = -A_p \rho_g \frac{K}{\mu}\frac{p - p_a}{y} \tag{26}$$

which is easy to solve

$$y(t)^2 = \frac{2K\rho_g}{\mu\rho_L}(p - p_a)(t - t_c) = 2\beta(t - t_c) \tag{27}$$

In this equation t_c is the critical time, when the liquid–gas interface enters the pore space or the linear region of mass loss ends. β is an abbreviation of

$$\beta = \frac{2K\rho_g}{\mu\rho_L}(p - p_a) \tag{28}$$

We insert the solution for $y(t)$ in the equation for the mass loss rate and obtain

$$\frac{dm}{dt} = -A_p \sqrt{\frac{K\rho_g\rho_L(p - p_a)}{2\mu}}\frac{1}{\sqrt{(t - t_c)}} \tag{29}$$

The loss rate does not decrease linear with time, but decreases continuously to zero with the inverse square root of drying time. Integration of Eq. (29) yields

$$m(t) = m_c - 2b\sqrt{(t - t_c)} \tag{30}$$

Here b is an abbreviation of

$$b = A_p \sqrt{\frac{K\rho_g\rho_L(p - p_a)}{2\mu}} \tag{31}$$

The kinetics of mass change with time is essentially determined by the permeability constant K. In nano- to mesostructured gels the permeability is the Knudsen permeability [27,28]. A derivation of this

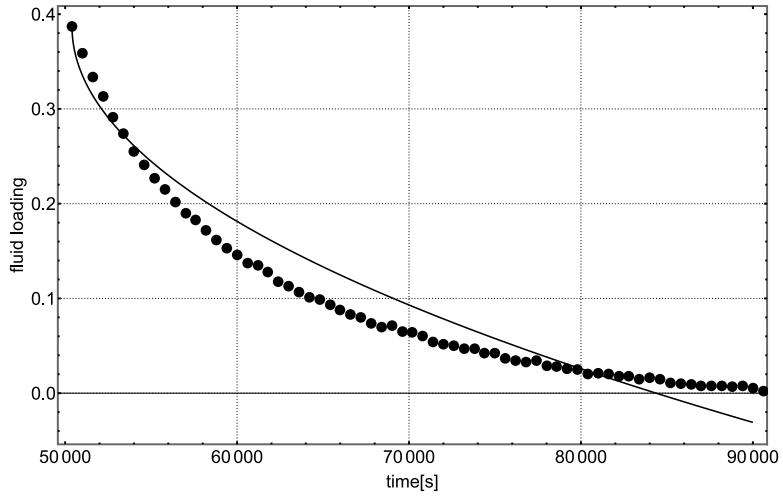

Fig. 9. Final phase of drying when the liquid–gas interphase has entered the pore space. The dots are the experimental values (sample of 30 mm thickness and dried at 80 °C), the solid line is a fit with Eq. (30).

equation is given in the appendix.

$$K_n = \frac{2d_p\mu}{3}\sqrt{\frac{M}{\pi RT}} \tag{32}$$

In macroporous materials various expressions for the permeability are available (for a collection of such expressions see the textbook of S.W. Churchill [29]). All expressions of the permeability in macroporous materials can described as

$$K_0(\phi_p, d_g) = g(\phi_p)d_g^2 \tag{33}$$

with d_g the particle size in the network, ϕ_p the volume fraction of pores, which is easily obtained from a measurement of the envelope and the skeletal density, see [1]. $g(\phi_p)$ is a function of porosity like the Kármán–Kozeny relation

$$g_{KK} = \frac{\phi_p^3}{150(1-\phi_p)^2} \tag{34}$$

or a simple arrangement of parallel cylinders and a Hagen–Poiseuille flow through them

$$g_{cyl} = \frac{\phi_p}{32} \tag{35}$$

Eq. (30) is fit to the experimental data using the non-linear fit procedure provided by Mathematica™. A result is shown in Fig. 9. The agreement is not so bad, but also not really convincing. One source of error might be that the model underestimates the liquid–gas area from which evaporation takes place. If we assume that the menisci look as shown schematically in Fig. 10 the surface area from which evaporation takes place is much larger. Here we have assumed that at the pore walls always a thin film of liquid exists (see [2]).

The shape of the evaporating surface as shown in Fig. 10 is greater than the simple model shown in Fig. 8. This additional surface is calculated by assuming that the film at the pore walls can be treated as a cylinder with diameter d_p, pore diameter and a height $y(t)$. If there are n_p pores the total evaporating surface is

$$A_V = A_p + \pi d_p y(t) n_p \tag{36}$$

We substitute this area into Eq. (29) by replacing A_p with A_V and obtain for the mass loss rate the expression

$$\frac{dm}{dt} = -(n_p\pi d_p y(t) + A_p)\frac{\rho_g K(p-p_a)}{\mu y(t)} = -\gamma - \frac{\epsilon}{\sqrt{2\beta(t-t_c)}} \tag{37}$$

Integrating this equation from m_c to $m(t)$ and t_c to t gives the mass as a function of time

$$m(t) = m_c - \gamma(t-t_c) - \sqrt{\frac{2\epsilon}{\beta}}\sqrt{t-t_c} \tag{38}$$

The abbreviations used are

$$\gamma = \pi n_p d_p \rho_g K(p-p_a) \quad \text{and} \quad \epsilon = \frac{A_p\rho_g K(p-p_a)}{\mu} \tag{39}$$

Note that in this case the vapour pressure above the curved liquid gas interface depends on the radius of curvature, expressed by the Kelvin equation.

$$p = p_{sat}\exp\left(-\frac{4\sigma V_m\cos\theta}{d_p RT}\right) \tag{40}$$

In this expression, σ is the interfacial tension of the liquid–gas interface, V_m is the molar volume, θ is the wetting angle, and R, T have their usual meaning. The Kelvin relation shows that the vapour pressure above a meniscus inside the pore network is reduced compared with the vapour pressure above a flat interface p_{sat}. Therefore, both constants γ, ϵ depend also on the interface tension. A non-linear fit of Eq. (38) to the experimental data is shown in 11. Compared to the simple model above, this fit is almost perfect. In order to describe the evaporation once the menisci have entered the pore space, it requires taking into account the liquid film formation at the pore walls and the evaporation from a much larger surface.

Let us check if the fit parameters are reasonable. Let us list the four parameters obtained from the non-linear fit with the model Eq. (38): $t_c = 49421$ s, $\sqrt{2\epsilon/\beta} = 0.0049$, $m_c = 0.53$, and $\gamma = 0.0000115$. The critical time and mass, denoting the deviation from the CRP phase, fit well to the experimental curve. The Kármán–Kozeny permeability is calculated as $3\cdot10^{-13}$ m^2. We can calculate the parameters if the number density of pores per area is known. Leaving this as a free parameter, a comparison with the fit parameters gives the number density of pores. We derive a value of $22\cdot 10^6$ per square meter. Although this means something like 22 pores per mm^2, the value is too low by probably a factor of 100. The calculated parameter $\sqrt{2\epsilon/\beta}_{\text{model}}$ is 0.1, and is thus a factor of 21 larger than the experimental value.

Although the model equation formally fits to the experimental part of the drying curves in the FRP phase, this agreement should not be overestimated, since the fit used four free parameters and, as shown above, two parameters do not fit to the expectations. We cannot expect, however, a perfect agreement between model and experiments, since we have neglected several issues: 1. The pores have different radii, such that the permeability changes in as much as the pores become dry; 2. $y(t)$ increases, since the tortuosity increases; 3. the pores are treated as cylinders, which they are not; 4. the pores are interconnected; 5. Wet patches can exist parallel to fully dried, liquid-free paths in the pore space; 6. The solid network deforms during drying and thus changes the pore geometry.

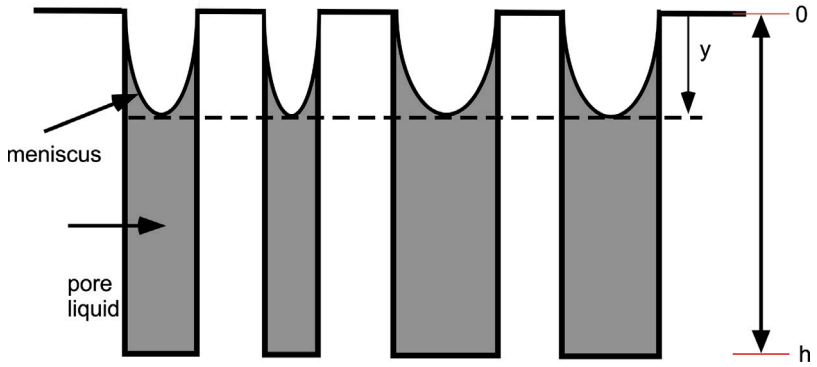

Fig. 10. Illustration of the liquid–gas interface (menisci) being drawn into the porous body by an amount $y(t)$ but here with a liquid film formation at the pore walls.

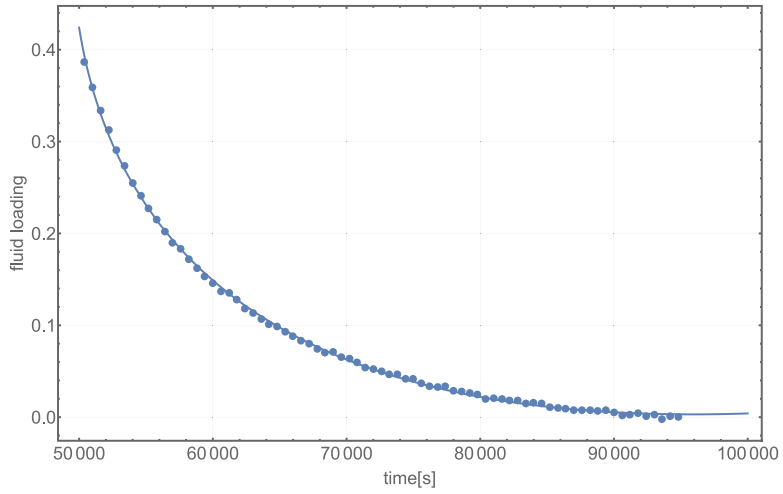

Fig. 11. Drying of porous RF-gels at 80 °C once the menisci have entered the pore space. The fit was made with Eq. (38) with four free parameters, m_c, t_c, γ and $\sqrt{\frac{2\epsilon}{\beta}}$.

A further improvement of the model should rely on better and more in-depth studies of the drying, including NMR and X-ray tomography, as done for macroporous, fluid filled packed beds of stone grains by Castell and co-workers [25,30] and Novak and co-workers [31]. The limits of the simple model ask for more sophisticated numerical modelling along the lines set by for instance Prat, Metzger, Haghighi, Kharaghani and recently by Nestler and her team employing phase field methods [7,13–17]. It should be mentioned that an improved modelling also should take into account the airflow dynamics in a drying cabinet.

5. Scales and shrinkage

In this section we will discuss a bit what are the parameters influencing the drying time and how one can accelerate drying. For the linear part of the drying curve we had derived Eq. (19). Inserting in that expression the terms for the boundary layer thickness and the Reynolds number lead to

$$t_e = \frac{5\rho_F L}{M D_g (c_s - c_a)} \frac{h}{\sqrt{Re}} \tag{41}$$

As to be expected, one can reduce the linear drying time by increasing the Reynolds number of the gas flow in a drying cabinet or reducing the thickness of the gel or increasing the temperature. In this relation is the specimen size also is important. We made a test of this prediction. We prepared an RF-gel according to the procedure mentioned above with different dimensions. The wet gel had a thickness of 10 mm, a length of 20.5 cm and a width of 27 cm. The measured drying curve is shown in Fig. 12 The comparison with the smaller sample first shows that the larger one needs longer to become fully dry. Performing to the linear part a least square fit gives a drying time in the CRP phase of 21.000 s. The smaller sample exhibited a linear drying time of 19144 s. The difference is only 10% and differs largely to the value of 58% from the prediction of Eq. (41). We must therefore conclude that the model overestimates the influence of sample size. It nevertheless shows that thickness is not the only relevant parameter, but the lateral shape is important too.

In the CRP phase of drying the liquid is squeezed by capillary forces to the gel surface and vice versa leads to a shrinkage of the gel. A rough estimate can be made with the bulk compression modulus of the gel K_{eff}. The deformation of the wet gel can be expressed by the following relation

$$\epsilon_V = -\frac{p}{3K_{eff}} \approx -\frac{p}{3K_s} \tag{42}$$

in which ϵ_V is the volumetric deformation strain (shrinkage), p the acting pressure of the fluid in the pore space and K_{eff} the compression modulus of the gel and K_s that of the solid network. In principle we have to describe the gel at least as a two phase material of a solid backbone and a viscous liquid. The interaction of the solid network and the motion of the fluid would have to be modelled. As a first guess one could ignore the fluid and take it simply as one that fills the pores and can easily be squeezed out of the pores by pressure similar to the behaviour of a wet sponge upon pressurisation. The average pressure in the pore space is the capillary pressure as expressed in Eq.

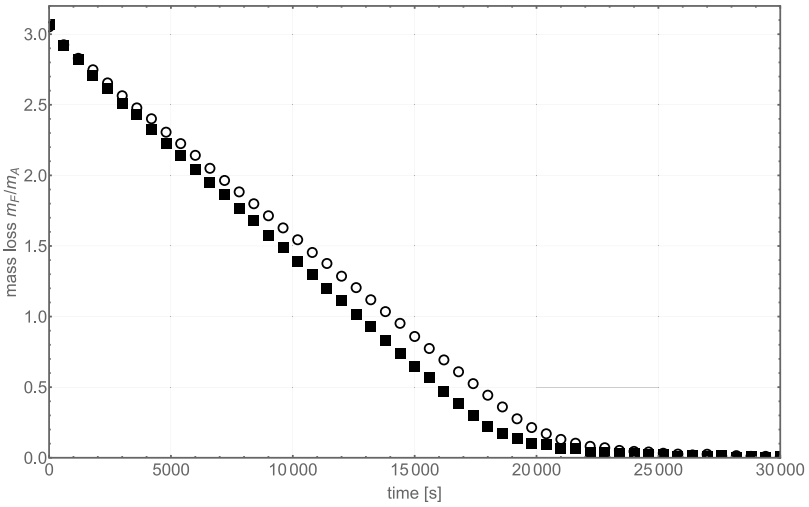

Fig. 12. Drying curve of an RF-gel at 80 °C. The full square show the mass loss of the sample with 13 cm length and the empty circles that of a sample with 20.5 cm edge length.

(40). The deformation strain depends for a given capillary pressure on the stiffness of the solid backbone K_s. The stiffer the backbone the smaller the deformation strain. In RF gels used in this study the total deformation in the lateral dimension was around 2.2% and 4.5% in volume. Thus the network is rather stiff and the change in pore size due to shrinkage will also be in the few percent range and therefore can be neglected.

6. Application to other aerogels

The simple model discussed above can be applied first to all types of gels not exhibiting a huge shrinkage, like all RF-gels with an R/C value above 500. Silica aerogels in which the surface is modified by hydrophobic groups are usually dried under ambient conditions, and although they shrink initially, they recover their shape fully [4]. The shrinkage pushes the pore liquid to the surface, especially during the CRP phase. But this is similar to squeezing a sponge. The developed model can also be applied to so-called marshmallow aerogels [32], since the microstructure is similar to those discussed here, besides that in these types of aerogels the particles are intrinsically flexible or rubber-like. Therefore, the model is applicable to all kinds of gels having pores in the range of 100 nm to a few microns and in which shrinkage is small or the solid network is stiff. For biopolymeric aerogels, like cellulose, alginates, chitosan the model cannot be applied, since in all these gels, deformation of the network is up to 80% [1].

7. Summary

A model is developed for drying wet gels with a solid network having pores in the range of 100 nm to micrometers. It concentrates on the evaporation from the wet gel into the gas phase above the gel accelerated by gas flow by, for instance, a fan in a drying cabinet. The model calculates the mass loss of a gel in the linear regime when the gel body is wet by the pore fluid due to capillary action and in the non-linear regime once the liquid enters the pore space in which the transport of vapour is dictated by the permeability of the pore space. The model fits the experimental data of resorcinol-formaldehyde gels. It also points to the fact that a better model is needed for the evaporation processes above a wet gel surface. Nevertheless, it makes at least semi-quantitative predictions on how to optimise drying of wet gels, leading to xero- or aerogels.

CRediT authorship contribution statement

Lorenz Ratke: Writing – original draft, Formal analysis. **Benjamin Ignatzi:** Investigation, Data curation, Conceptualization.

Declaration of competing interest

The authors declare that they have no known competing financial interests or personal relationships that could have appeared to influence the work reported in this paper.

Appendix. Knudsen permeability

Let us consider a nano- to mesoporous solid. If a gas flow through such a body would be driven by a pressure gradient one can apply Darcy's law. The gas flow velocity v is

$$v = -\frac{K_n}{\mu}\nabla p \tag{A.1}$$

in which K_n denotes the Knudsen permeability. If the gas flow is driven by a concentration gradient, one can use Fick's first law to obtain the flow rate j

$$j = -D_k \nabla c \tag{A.2}$$

We now apply the ideal gas law

$$c = \frac{p}{RT} \tag{A.3}$$

and use $j = c \cdot v_D$ to obtain

$$c \cdot v_D = \frac{D_k}{RT}\nabla p \tag{A.4}$$

Rearranging gives

$$v_D = \frac{D_k}{cRT}\nabla p \tag{A.5}$$

Compare this with Darcy's law yields

$$\frac{K_n}{\mu} = \frac{D_k}{cRT} \tag{A.6}$$

or simply

$$K_n = D_k \frac{\mu}{cRT} = D_k \frac{\mu M}{\rho RT} \tag{A.7}$$

Whereas c is the gas density in mole/m^3, ρ is the gas density in kg/m^3. Using the well known expression for the Knudsen diffusivity

$$D_k = \frac{2d_p}{3}\sqrt{\frac{RT}{\pi M}} \tag{A.8}$$

leads to Eq. (32). One should recognise that usually the permeability of a porous body is only a geometric quantity and does not depend on physical properties of the moving fluid but only on the characteristics

of the pore space. The result derived above in Eq. (A.7) shows that the diffusivity and the density of the gas are important. Note also that μ/ρ is the kinematic viscosity, which is equal to the gas diffusivity (not the Knudsen diffusivity).

References

[1] L. Ratke, P. Gurikov, The Chemistry and Physics of Aerogels, Cambridge University Press, Cambridge, UK, 2021.
[2] C.J. Brinker, G.W. Scherer, Sol-Gel Science: The Physics and Chemistry of Sol–Gel Processing, Academic Press, Inc, San Diego, 1990.
[3] J. Crank, The Mathematics of Diffusion, second ed., Clarendon Press, Oxford, UK, 1975.
[4] A. Bisson, E. Rodier, A. Rigacci, D. Lecomte, P. Achard, Study of evaporative drying of treated silica gels, J. Non-Cryst. Solids 350 (2004) 230–237.
[5] R. Brandt, R. Petricevic, H. Pröbstle, J. Fricke, Acetic acid catalyzed carbon aerogels, J. Porous Mater. 10 (2003) 171–178.
[6] R. Petricevic, G. Reichenauer, V. Bock, A. Emmerling, J. Fricke, Structure of carbon aerogels near the gelation limit of the resorcinol-formaldehyde precursor, J. Non-Cryst. Solids 225 (1998) 41–45.
[7] E. Haghighi, Evaporation from porous surfaces into turbulent airflows, (Ph. D. thesis), ETH Zürich, 2015.
[8] T. Kudra, A.S. Mujumdar, Advanced Drying Technologies, second ed., CRC Press, Taylor and Francis Group, Boca Raton, FL, USA, 2009.
[9] B. Kulkarni, H.T. Vu, E. Tsotsas, Mass and heat transport models for analysis of the drying process in porous media: A review and numerical implementation, Int. J. Chem. Eng. 2 018 (2018) 9456418.
[10] S.T. Pham, DEM-based triangulation pore network model for particle aggregates: Drying and capillary forces, (Ph. D. thesis), Otto-von-Guericke-Universität, 2021.
[11] O. Borgman, P. Fantinel, L. Goehring W. Lühder, R. Holtzman, Impact of spatially correlated pore-scale heterogeneity on drying porous media, Water Resour. Res. 53 (7) (2017) 5645–5658.
[12] Z. Lu, I. Kinefuchi, K.L. Wilke, G. Vaartstra, E.N. Wang, A unified relationship for evaporation kinetics at low mach numbers, Nat. Commun. 10 (1) (2019) 2368.
[13] M. Prat, Recent advances in pore-scale models for drying of porous media, Chem. Eng. J. 86 (2002) 153–164.
[14] M. Prat, On the influence of pore shape, contact angle and film flows on drying of capillary porous media, Int. J. Heat Mass Transfer 50 (2007) 1455–1468.
[15] T. Metzger, M. Kwapinski, M. Peglow, G. Saage, E. Tsotsas, Modern modelling methods in drying, Transp. Porous Media 66 (2007) 103–120.
[16] A. Kharaghani, Drying and wetting of capillary porous materials: Insights from imaging and physics-based modeling, habilitationsschrift, Otto-von-Guericke-Universitat, Magdeburg, 2020.
[17] M. Weichel, M. Reder, S. Daubner, J. Klemens, D. Burger, P. Scharfer, W. Schabel, B. Nestler, D. Schneider, Modeling the drying process in hard carbon electrodes based on the phase-field method, Phys. Rev. Mater. 9 (2025) 035403.
[18] B. Krasovitov, A. Fominykh, S. Wolf, C. Schilde, A. Levy, Modeling porous shell formation in bidisperse suspension droplet drying, Dry. Technol. (2025) 1–13.
[19] M. Lippke, T. Ohnimus, F. Frankenberg, C. Schilde, A. Kwade, Drying and calendering of lithium ion battery electrodes: A combined simulation approach, Powder Technol. 444 (2024) 119984.
[20] S. Whitaker, Simultaneous heat, mass, and momentum transfer in porous media: A theory of drying, in: *Adavnces in Heat Transfer*, Vol. 13, Academic Press, Inc., New York, 1977, pp. 119–203.
[21] S. Whitaker, W.T.-H. Chou, Drying granular porous media - theory and experiment, Dry. Technol. 1 (1) (1983) 3–33.
[22] V. Levich, Physicochemical Hydrodynamics, Prentice Hall, Englewood Cliffs, NJ, 1962.
[23] H. Schlichting, K. Gersten, Boundary-Layer Theory, Eighth ed., Springer, Berlin, Berlin, 2003.
[24] J. van Brakel, Mass transfer in convective drying, in: Advances in Drying, vol. 1, pp. 217–267.
[25] R. Le Dizès Castell, L. Pel, T. Chekai, H. Derluyn, M. Scheel, S. Jabbari-Farouji, N. Shahidzadeh, Sol–gel transition by evaporation in porous media, Phys. Rev. Appl. 21 (2024) 034049.
[26] B. Ignatzi, Entwicklung eines energieoptimierten konzeptes zur trocknung von resorcin-formaldehyd-aerogelen (Master's thesis), Rheinische Fachhochschule Köln, 2022.
[27] F. Javadpour, Nanopores and apparent permeability of gas flow in mudrocks (shales and siltstone), J. Can. Pet. Technol. 48 (08) (2009) 16–21.
[28] Yoshiaki Kawagoe, Tomoya Oshima, Ko Tomarikawa, Takashi Tokumasu, Tetsuya Koido, Shigeru Yonemura, A study on pressure-driven gas transport in porous media: from nanoscale to microscale, Microfluid. Nanofluidics 20 (2016) 162.
[29] S.W. Churchill, Viscous flows, in: Butterworths Series in Chemical Engineering, Butterworths Publishers, Stoneham, MA, 1988.
[30] R. Le Dizès Castell, M. Prat, N. Shahidzadeh, S. Jabbari-Farouji, Pore network modeling for evaporation of complex fluids in porous media, Phys. Rev. Fluids 10 (2025) 094302, http://dx.doi.org/10.1103/bq4n-j2yb, https://link.aps.org/doi/10.1103/bq4n-j2yb.
[31] V. Novak, M. Blazek, P. Koci C. m. Schlepütz, M. Stamponi, Drying of water from porous structures investigated by time-resolved x-ray tomography, Dry. Technol. 40 (2022) 3675–3693.
[32] K. Kanamori, M. Aizawa, K. Nakanishi, T. Hanada, New transparent methylsilsesquioxane aerogels and xerogels with improved mechanical properties, Adv. Mater. 19 (2007) 1589–1593.